Available online at www.sciencedirect.com
SCIENCE DIRECT
International Journal of Mechanical Sciences 48 (2006) 799–808
International Journal of MECHANICAL SCIENCES
www.elsevier.com/locate/ijmecsci

Plastic collapse of thin-walled frusta and egg-box material under shear and normal loading

A.R. Akisanya[a,*], N.A. Fleck[b]

[a]School of Engineering and Physical Sciences, University of Aberdeen, Fraser Noble Building, Aberdeen, Scotland AB24 3UE, UK
[b]Department of Engineering, University of Cambridge, Trumpington Street, Cambridge CB2 1PZ, UK

Received 17 September 2004; received in revised form 12 December 2005; accepted 28 January 2006
Available online 20 March 2006

Abstract

The quasi-static plastic collapse of thin-walled frusta is determined for combined shear and out-of-plane compression. Experiments and finite element calculations are conducted on conical metallic frusta with semi-included cone angles of 30° and 45° to determine the shear collapse response. Additional finite element predictions are given for compressive loading, and for combined shear-compressive loading. The dependence of strength and energy absorption upon geometry is explored. The predicted response of an array of conical frusta is used to give the overall response of an egg-box material sandwiched between rigid face sheets. Scaling laws are determined for the stiffness and strength as a function of relative density of the egg-box material.

Keywords: Plastic collapse; Energy absorption; Egg-box material; Conical frusta

1. Introduction

There is a continued need to develop crashworthy structures for transport applications. Energy absorbers include thin-walled tubes, shells and metallic foams; they are usually designed for predominantly compressive loading and function by converting kinetic energy into irreversible plastic work. Ideally, they should possess additional functions such as sound and vibration absorption, and provide local stiffening to increase the frequency of natural modes of vibration (such as for the pillars and struts of an automobile chassis). A challenging opportunity exists in developing and optimising new types of energy absorbing system.

The deformation and energy absorbing characteristics of thin-walled tubes, frusta and metallic foams under axial compressive loading have been extensively studied; see for example [1–4]. Typically, energy is absorbed by the activation of plastic hinges and the amount of energy absorbed is a function of the material properties, rate of loading, shape of the energy absorber and of the resulting collapse mechanism. This relationship is summarised for different energy absorbers and types of loading in the review papers of Reid [5] and Alghamdi [6], and in the recent book by Ashby et al. [4]. Consider, for example, the bending collapse of thin-walled tubes as addressed by Mamalis et al. [7] and Kecman [8]. For tubes of circular cross-section, a critical diameter-to-thickness ratio exists for which the energy absorbing capacity of the tube is a minimum [7]. Recently, Chen et al. [9] have analysed the bending collapse of sandwich beams with a metallic foam core. The dominant mode of collapse by face yield, indentation or core shear was found to depend upon the ratio of face sheet to core thickness, and upon the ratio of core thickness to span of the beam [9].

It is clear from a search of the literature that the response of energy absorbing systems to shear loading and combined compressive-shear loading has received little attention. This is somewhat surprising, as the cores of sandwich structures are commonly loaded in shear. The buckling of circular cylindrical shells subjected to transverse shear has been investigated by Galletly and Blachut [10], Matsuura et al. [11] and Athiannan and Palaninathan

*Corresponding author. Tel.: +44 1224 272 989; fax: +44 1224 272 497.
E-mail address: a.r.akisanya@eng.abdn.ac.uk (A.R. Akisanya).

0020-7403/$ - see front matter © 2006 Elsevier Ltd. All rights reserved.
doi:10.1016/j.ijmecsci.2006.01.020

[12]. In the current paper the deformation and energy absorbing characteristics of conical frusta subjected to shear loading are determined, and the results are used to predict the collapse response of an egg-box material to shear loading. The energy absorption of conical frusta and egg-box panels subjected to uniaxial compression has recently been determined by Deshpande and Fleck [13] and Zupan et al. [14]. Three collapse modes were identified depending upon the imposed constraints: (i) travelling hinge mechanism for a constrained egg-box panel with no face sheets, (ii) inversion of the truncated cone followed by axisymmetric plastic buckling when the egg-box panel is unconstrained laterally and has no face sheets, and (iii) axisymmetric plastic buckling of an egg-box panel with bonded face sheets, such that lateral straining is prevented. The experimental and finite element results of Zupan et al. [14] and the theoretical results of Deshpande and Fleck [13] showed that the energy absorption per unit volume of egg-box panels under uniaxial compression exceeds that of metallic foams, and the travelling hinge mechanism gives the highest energy absorption.

In this study, the collapse response and energy absorbing characteristics of a conical frustum subjected to transverse shear are examined. A sketch of a typical conical frustum is given in Fig. 1. The frustum has top and base diameters of $2a$ and $2b$, respectively, a height h, wall thickness t, and cone angle ω, as defined in the figure. The top and bottom faces of the frusta are subjected to a relative shear displacement u_1; the work-conjugate shear force S is determined experimentally and by the finite element method, for two cone angles ($\omega = 45^\circ$ and 60°) and for two wall thicknesses ($t = 0.3$ and 0.5 mm). The finite element method is used to explore the sensitivity of the collapse response to geometry, and to predict the combined shear and collapse response of an egg-box material consisting of a square array of conical frusta.

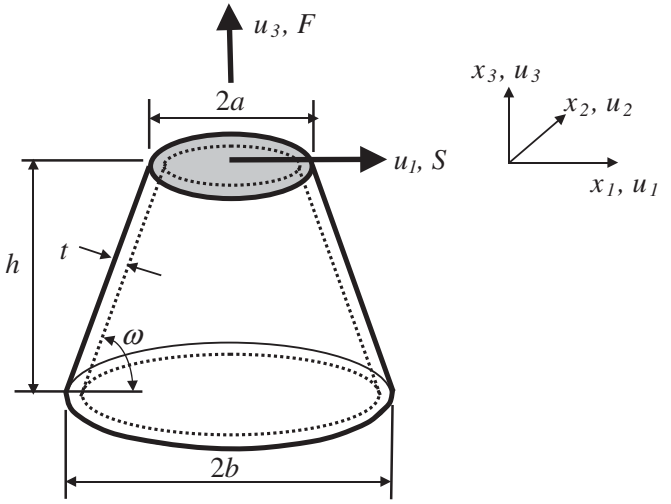

Fig. 1. A schematic of a conical frustum subjected to transverse shear load S parallel to the co-ordinate axis x_1 and to normal load F parallel to the co-ordinate axis x_3. u_1, u_2 and u_3 are displacements along the Cartesian axes x_1, x_2 and x_3, respectively.

2. Shear collapse experiments

2.1. Test material and experimental procedure

A series of shear collapse experiments has been conducted on conical frusta. The frusta were made from brass (composition 60% copper, 40% zinc by weight) for ease of manufacture and for its high ductility. The uniaxial stress versus strain response of the as-received brass was measured at a strain rate of $10^{-3}\,s^{-1}$ using a dog-bone specimen (gauge section of length 30 mm, width 13.4 mm and thickness 1 mm). The stress versus strain responses of three nominally identical brass specimens were identical to within a few percent, and a representative uniaxial stress versus strain response is given in Fig. 2. The average modulus, 0.1% offset yield strength and ultimate tensile strength were 76 GPa, 200 MPa and 386 MPa, respectively, while the elongation to failure was 12%. The measured uniaxial stress–strain response has been curve-fitted by the piecewise linear–power law hardening relation

$$\frac{\sigma}{Y} = \begin{cases} \varepsilon/\varepsilon_y & \text{for} \quad \varepsilon \leqslant \varepsilon_y, \\ (\varepsilon/\varepsilon_y)^n & \text{for} \quad \varepsilon > \varepsilon_y, \end{cases} \tag{1}$$

where n is the hardening index, and Y and ε_y are the uniaxial yield strength and yield strain, respectively. The power law relation (1) adequately predicts the measured stress–strain response for the choice $n = 0.2$, $Y = 200$ MPa and $\varepsilon_y = 0.3\%$, as shown by the curve fit in Fig. 2.

Conical frusta were machined from a brass rod of diameter 50 mm. The top of each frustum has an extended solid rod of diameter $2a$ (= 10 mm) to allow for application of a shear force, while the base of each frustum was machined into a cylindrical tube (see Fig. 3). It is emphasised that the top solid rod, the frustum and the cylindrical tube were machined as a single unit. The test arrangement was such that the frustum was subjected to a shear displacement u_1 parallel to the x_1 axis, with zero axial

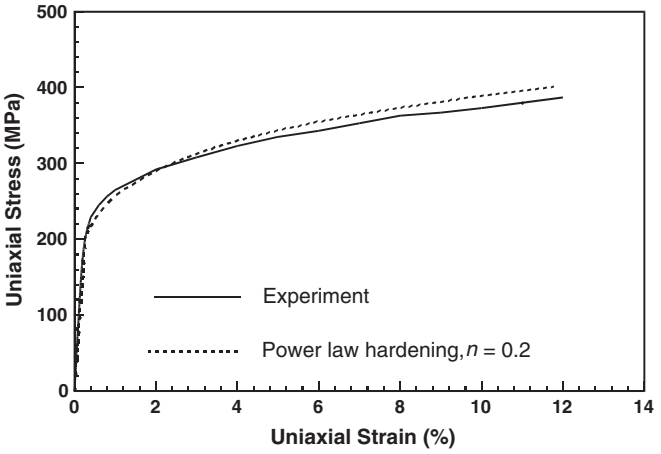

Fig. 2. Measured uniaxial stress versus strain response of the test material, 60/40 brass, and a power-law idealised response with yield strain $\varepsilon_y = 0.3\%$, initial flow stress $Y = 200$ MPa and strain hardening index $n = 0.2$.

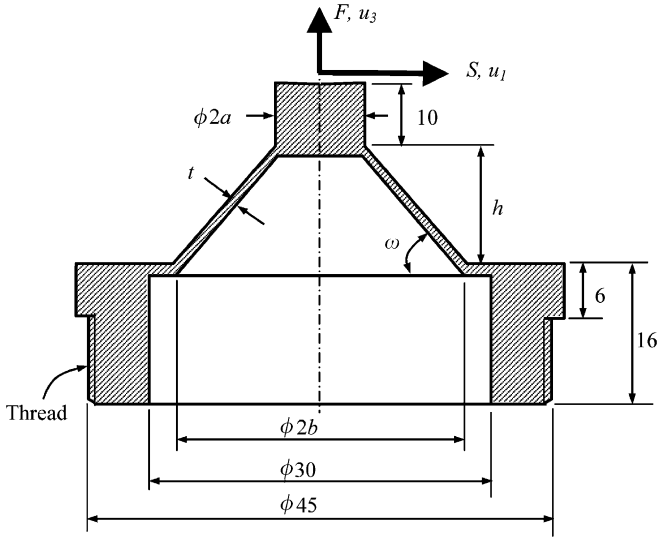

Fig. 3. Cross-sectional geometry (not to scale) of a conical frustum subjected to shear load S and normal load F, as used in the experiment. All dimensions are in millimetres.

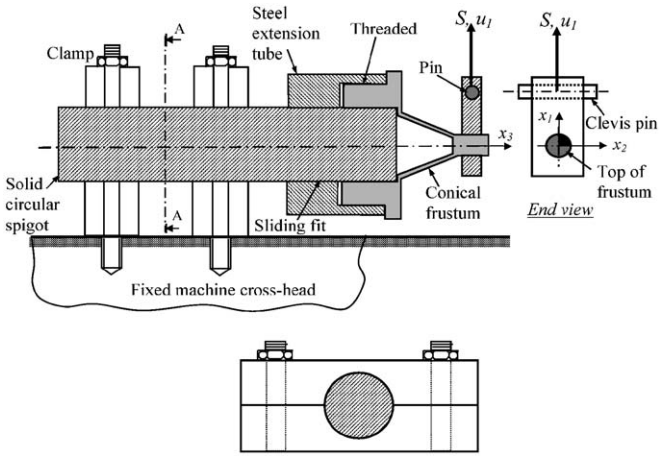

Fig. 4. The loading arrangement used in the shear tests on conical frusta; x_1, x_2 and x_3 are the Cartesian co-ordinate axes used to describe the applied loads and the deformation of the frusta.

force parallel to the x_3 axis and full constraint against rotation of the ends of the frustum about the x_2 axis; these co-ordinate axes are defined in both Figs. 1 and 4. The cylindrical tube at the base of each frustum was externally threaded (M45 × 10 mm) in order to screw the base of the specimen into an internally threaded steel extension tube, as shown by the assemblage of specimen and grips in Fig. 4. In turn, the steel extension tube was allowed to slide freely on a steel spigot, and the spigot was clamped to the bed of the screw-driven test machine, see Fig. 4. The top of the frustum was loaded transversely by the moving crosshead of the test machine using a clevis pin.

The shear tests were performed at a displacement rate of $0.017\,\mathrm{mm\,s^{-1}}$, and both the crosshead displacement and the load were continuously recorded using a data logger. Two cone angles were considered, $\omega = 45^\circ$ and 60°, and the nominal thickness of the cones was $t = 0.3$ and 0.5 mm. All specimens had a top radius $a = 5$ mm and a height $h = 10$ mm. Attempts were made to machine conical frusta with a wall thickness below 0.3 mm, but these were not successful because the frusta failed by local buckling during the machining operation. Table 1 contains a summary of the specimen geometries employed.

2.2. Measured collapse response in shear

The measured shear force versus displacement responses are shown in Fig. 5. The initial elastic response is followed by a strain hardening plastic behaviour and then by plastic buckling in the vicinity of peak load, as indicated by an arrow in the respective force versus displacement curves of Fig. 5. An appreciation of the buckling mode is given by photographs of the diametral sections of the tested specimens, as shown in Fig. 6(a) for the choice $t = 0.5$ mm, $\omega = 45^\circ$ and in Fig. 6(b) for $t = 0.5$ mm, $\omega = 60^\circ$. In the post-buckling regime, the conical portion opposite the buckled zone undergoes tensile stretching as shown in Figs. 6(a) and 6(b). The tests were terminated at the onset of tearing. Both the buckling load and the shear displacement at the onset of tearing increase with increasing wall thickness, see Table 1. In contrast, with increasing cone angle, the buckling load decreases while the displacement at tear initiation increases.

3. Numerical simulations

A 3D finite element analysis of the deformation response of conical frusta subjected to shear loading was carried out using the finite element package ABAQUS Standard [15]. The as-machined local shape at the junction of the flat top of diameter $2a$ and the conical portion of the frustum was given a fillet of radius 2 mm, as measured by Deshpande and Fleck [13]. In all cases the top of the frusta was closed and flat, with a radius of $a = 5$ mm and a height $h = 10$ mm. Each frustum was modelled by 2088 four-noded shell elements (S4 in ABAQUS). The base of the frusta was fully constrained against lateral motion and rotation, while the top of the frusta was constrained against rotation about any axis, and against lateral motion u_2 parallel to the x_2 axis; recall that the co-ordinate system has already been defined in Fig. 1. The shear response was determined by prescribing a shear displacement u_1 to all nodes of the frusta top, with unconstrained axial motion u_3 of the flat top. J2 flow theory was employed, with isotropic hardening for an elastic/power-law hardening solid. The Poisson's ratio as taken as $\nu = 0.3$, and the yield strain was held fixed at $\varepsilon_y = 0.3\%$. First, we present results for a material with a hardening index $n = 0.2$ and yield strength $Y = 200$ MPa, representative of that for brass. The sensitivity of the collapse response to the hardening index n was subsequently examined for selected geometries.

Numerical stability and the removal of a plastic bifurcation was assured by imposing a small initial

Table 1
Specimen geometry, measured buckling load, and shear displacement at the initiation of tearing for the conical frusta

Cone angle (ω, deg)	Sample code	b (mm)	a (mm)	h (mm)	t (mm)	a/h	a/t	Buckling load (kN)	Displacement at tearing (mm)
45	S1	15	5	10	0.3	0.5	16.7	2.12	1.79
45	S2	15	5	10	0.3	0.5	16.7	2.10	2.42
45	S2	15	5	10	0.5	0.5	10.0	4.50	2.03
45	S4	15	5	10	0.5	0.5	10.0	3.03	3.06
60	S5	10.8	5	10	0.3	0.5	16.7	1.92	2.64
60	S6	10.8	5	10	0.3	0.5	16.7	2.20	1.58
60	S7	10.8	5	10	0.5	0.5	10.0	2.96	3.43

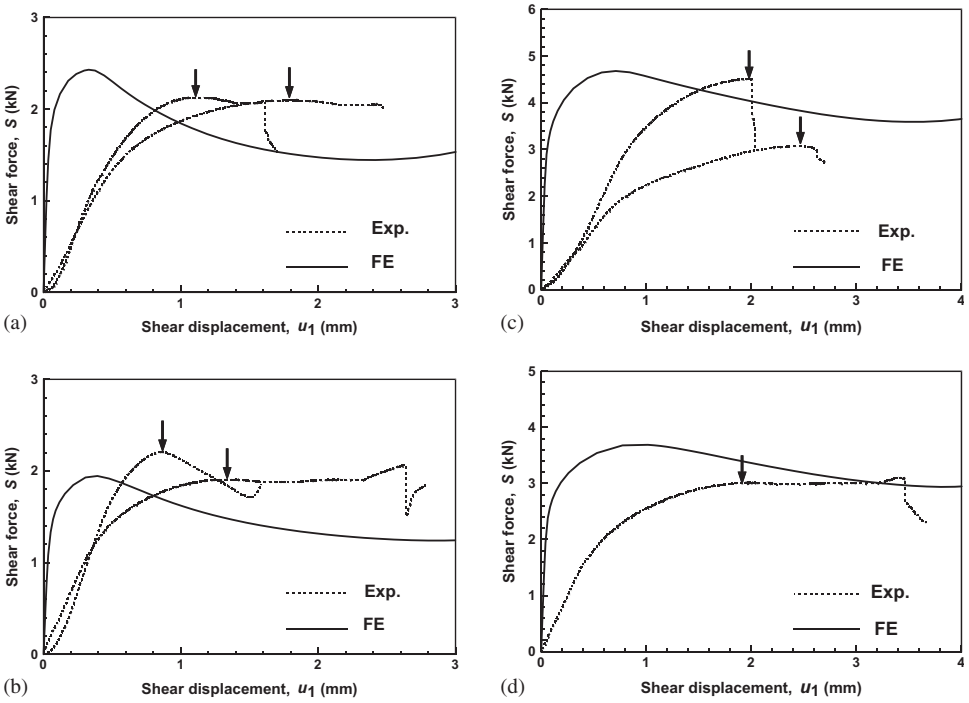

Fig. 5. Measured and predicted shear force, S, versus displacement, u_1, response for conical frusta made from brass and of height $h = 10$ mm. (a) Wall thickness $t = 0.3$ mm and cone angle $\omega = 45^\circ$, (b) $t = 0.3$ mm and $\omega = 60^\circ$, (c) $t = 0.5$ mm and $\omega = 45^\circ$, and (d) $t = 0.5$ mm and $\omega = 60^\circ$. The arrows on the measured response indicate the onset of plastic buckling.

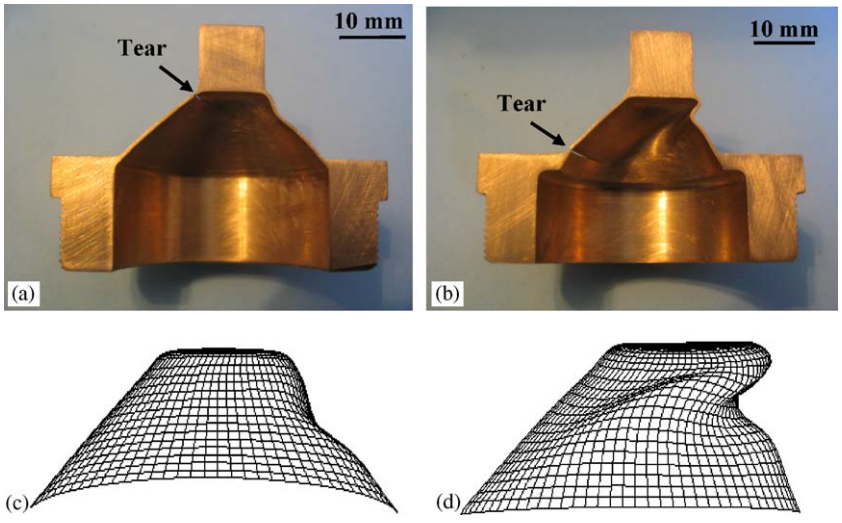

Fig. 6. The cross-section of the measured collapsed mode of conical frusta tested in shear for a conical angle of (a) $\omega = 45^\circ$ and (b) $\omega = 60^\circ$, and the corresponding finite element predicted collapsed mode for (c) $\omega = 45^\circ$ and (d) $\omega = 60^\circ$. All the specimens shown have a wall thickness of $t = 0.5$ mm, height $h = 10$ mm and flat top radius of $a = 5$ mm.

geometric imperfection to the initial shape, as follows. A preliminary elastic buckling analysis was used to define the initial imperfection: it is well known that imperfections based upon elastic buckling modes are useful for the analysis of plastic buckling of structure, see for example Athiannan and Palaninathan [12]. A representative eigenmode used for the shape of the imperfection is given in Fig. 7(a); it relates to a frustum of geometry $\omega = 45^\circ$, $a/t = 10$ and $a/h = 0.5$. A nonlinear finite element analysis of the imperfect frusta was then performed using the Riks algorithm and the elastic/power-law hardening response (1).

The sensitivity of the shear response to the magnitude of imperfection is shown in Fig. 7(b) for a frustum of geometry $\omega = 45^\circ$, $a/h = 0.5$ and $t = 0.5$ mm, and made from an elastic/power-law hardening solid of yield strain $\varepsilon_y = 0.3\%$, yield strength $Y = 200$ MPa and hardening index $n = 0.2$. The shear force S has been normalised by Yta where t is the wall thickness and a ($= 5$ mm) is the outer radius of the top of the frustum. The shear displacement u_1 has been normalised by the height h. Note that the shear response is relatively insensitive to the magnitude of initial geometric imperfection provided the maximum transverse displacement associated with the imperfection is less than the wall thickness: the shear buckling load for a frustum containing an imperfection equal to the wall thickness is only 15% below that for a perfect frustum. A similar level of sensitivity to the magnitude of imperfection on the shear collapse load has been observed experimentally for circular cylindrical shells [10,12]. Galletly and Blachut [10] measured the shear-buckling load for steel circular cylinders, and then repeated the test on the buckled specimens by reversing the direction of loading. The shear-buckling load for the second test was only 10% lower than that from the first test. Athiannan and Palaninathan [12] carefully measured the magnitude and location of the geometric imperfection in circular cylindrical shells prior to conducting a transverse shear test. Their experimental results showed that the magnitude of geometric imperfection has a marginal effect upon the shear collapse load for imperfections on the order of three times the wall thickness of the cylinder. In the present study, the maximum transverse distortion in shape associated with the imperfection was chosen to be 10% of the wall thickness for all conical frusta subjected to shear loading.

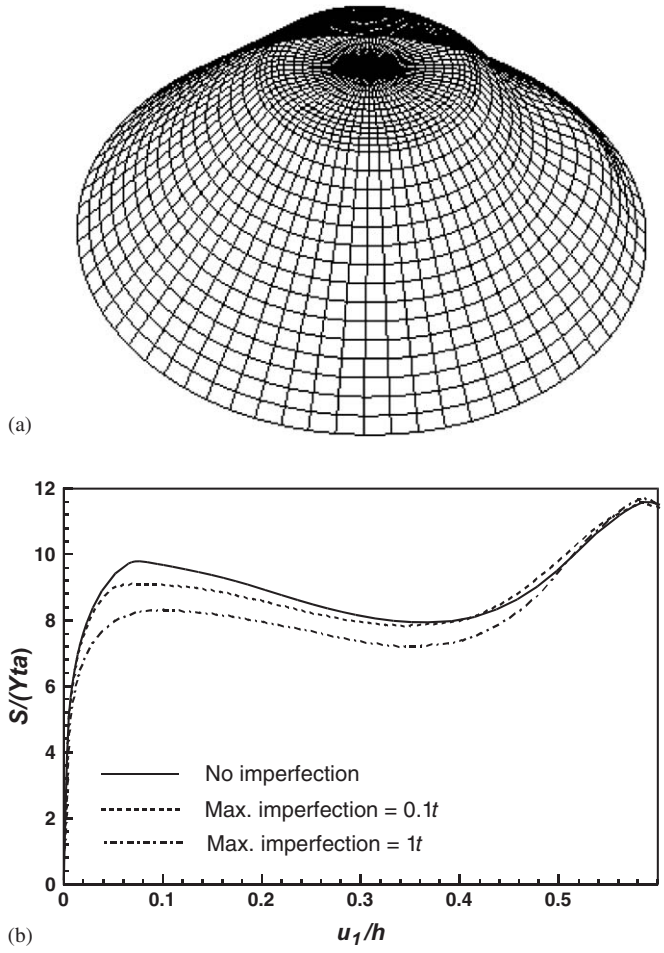

Fig. 7. (a) The eigenmode shape used for introducing geometric imperfection to the conical frusta loaded in shear. (b) Effect of the magnitude of geometric imperfection on the shear force, S, versus displacement, u_1, response of a conical frustum with cone angle $\omega = 45^\circ$ and wall thickness $t = 0.5$ mm, and made from a power-law hardening solid with yield strain $\varepsilon_y = 0.3\%$ and hardening index $n = 0.2$. The shear force has been normalised by Yta where Y ($= 200$ MPa) is the yield strength of the solid, and the displacement has been normalised by the height h ($= 10$ mm).

The predicted shear force versus shear displacement response is included in Fig. 5 for a conical frustum of wall thickness $t = 0.3$ and 0.5 mm. The numerical results shown in Fig. 5 are for elastic/power-hardening solid with material parameters identical to those experimentally determined for the brass material: $\varepsilon_y = 0.3\%$, $Y = 200$ MPa and $n = 0.2$. The predicted response is significantly stiffer than the measured response due to unavoidable slop in the test fixture (see Fig. 4). Similar discrepancies between the measured and predicted stiffness has been reported for the compressive response of egg-box material made from an array of conical frusta, see Zupan et al. [14]. Both the measured and predicted shear force versus displacement responses of the brass conical frusta show an initial peak, corresponding to the initiation of plastic buckling, accompanied by a subsequent drop in load in the post-buckling regime.

The predicted dependence of the normalised initial peak shear force, $S_{\max}/(Yta)$, upon the normalised wall thickness, t/a, is in reasonable agreement with the measured response, see Fig. 8. It is evident that the peak load increases with increasing relative wall thickness, t/a, and with decreasing cone angle ω.

For comparison purposes, the buckling mode predicted by the finite element simulations is included in Figs. 6(c) and (d) for frusta with wall thickness $t = 0.5$ mm, $a/h = 0.5$ and cone angle $\omega = 45^\circ$ (Fig. 6(c)) and $\omega = 60^\circ$ (Fig. 6(d)). Recall that h is the height of the frustum and a is the radius

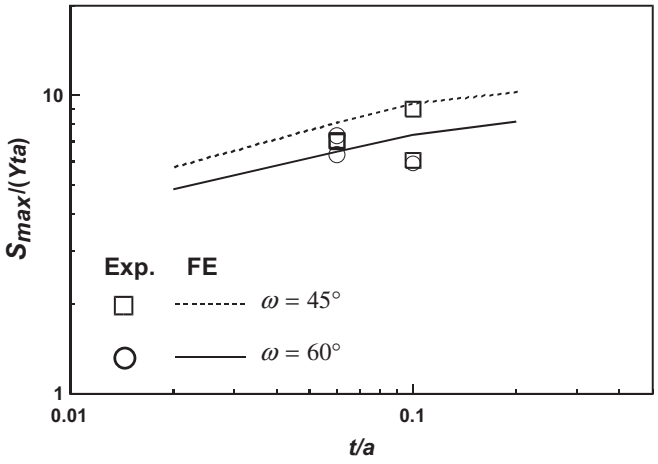

Fig. 8. Comparison of the measured and predicted initial maximum shear force S_{max} versus wall thickness t, for conical frusta with a flat top radius $a = 5$ mm. The maximum shear force has been normalised by Yta where Y ($= 200$ MPa) is the uniaxial yield strength of the material, while the thickness has been normalised by the top radius a. The finite element results are for a power-law hardening solid with a yield strain of 0.3% and strain hardening index $n = 0.2$.

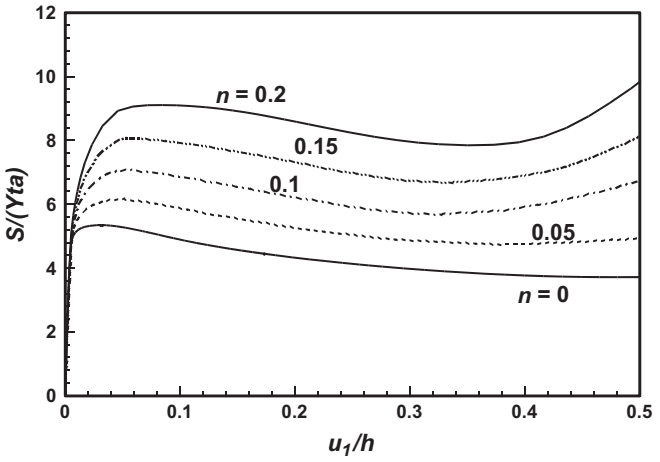

Fig. 9. The effect of strain hardening index n on the shear force versus displacement response for conical frusta with flat top radius $a = 5$ mm, height $h = 10$ mm and cone angle $\omega = 45°$. The shear force has been normalised by Yta where Y is the initial uniaxial flow stress of the material, while the displacement has been normalised by the height h. The numerical results are for a power-law hardening solid with a yield strain of 0.3%.

of the flat top; $a = 5$ mm in all cases considered. The predicted buckling mode is similar to the experimentally observed buckling mode (recall Figs. 6(a) and (b)). In the post-buckling regime a crease develops, and significant stretching occurs in the conical portion behind the plastic hinge. This leads to the observed tearing, as shown in Figs. 6(a) and (b).

The role of the hardening index n upon the shear collapse response of a conical frustum is examined using the finite element method. The frustum considered has a top radius $a = 5$ mm, height $h = 10$ mm, cone angle $\omega = 45°$ and wall thickness $t/a = 0.1$. The uniaxial stress–strain response of the material is given by the elastic/power-law relation (1) with Poisson's ratio $v = 0.3$, yield strain $\varepsilon_y = 0.3\%$, and the strain hardening index n is given selected values in the range $0 \leqslant n \leqslant 0.2$. J2 flow theory with isotropic hardening was assumed and a geometric imperfection in the shape of the linear buckling mode shown in Fig. 7(a) was imposed on the perfect frustum; the maximum transverse displacement of the imperfection was taken as 10% of the wall thickness. The predicted normalised shear force versus shear displacement response is shown in Fig. 9. The shear force versus shear displacement response is qualitatively similar for all values of the hardening index n considered: an initial elastic response is followed by a strain hardening plastic behaviour and then by plastic buckling in the vicinity of peak load. The shear collapse load (i.e. the first peak force) increases with increasing value of the strain hardening index, n; for example, the normalised shear collapse force for $n = 0.2$ (appropriate for brass) is about 75% greater than that for an elastic-ideally plastic solid ($n = 0$). The collapse mode for all values of n considered is qualitatively similar to that shown in Fig. 6 for $n = 0.2$.

4. Implications for egg-box material

4.1. Description of the geometry

The shear force versus displacement response of conical frusta can be used to deduce the collapse response and energy absorption characteristics of an egg-box material. Consider an egg-box material of depth $2h$ made from a metal sheet of thickness t, as sketched in Fig. 10. The egg-box geometry can be approximated by a square array of conical frusta and adjacent inverted frusta, each with top diameter $2a$, cone angle ω and height h. The unit cell for each frustum is assumed to have a height $2h$ and a square base of side $(2a + 2h \cot \omega)$. The relative density, $\bar{\rho}$, of the egg-box material, defined as the ratio of the density of the egg-box material to the density of the solid material from which it is made, is given by

$$\bar{\rho} = \frac{\pi}{8}\bar{t}\left[\frac{\bar{a}^2\bar{t}^2 \sin \omega + 2\bar{a}\bar{t} + \cot \omega}{\sin \omega(\bar{a}\bar{t} + \cot \omega)^2}\right], \tag{2}$$

where $\bar{a} = a/t$ and $\bar{t} = t/h$.

Each unit cell of the egg-box consists of a conical frustum, and the average shear stress, τ, and normal stress, σ, on the face of the egg-box material subjected to a shear force S parallel to the x_1 axis, and to a normal force F parallel to the x_3 axis are given by

$$\tau = \frac{S}{4(a + h \cot \omega)^2} \tag{3}$$

and

$$\sigma = \frac{F}{4(a + h \cot \omega)^2}, \tag{4}$$

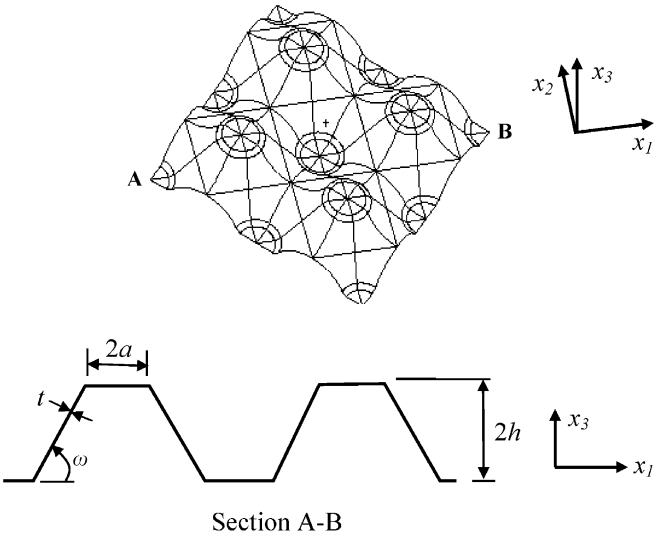

Fig. 10. Sketch of egg-box material. It comprises an arrangement of frusta and inverted frusta, each of height h. x_j ($j = 1, 3$) are Cartesian co-ordinate axes used to describe the geometry and the deformation.

where x_j ($j = 1, 3$) are the Cartesian axes shown in Fig. 10. The nominal shear strain and normal strain are $\gamma = u_1/h$ and $\varepsilon = u_3/h$, where $2u_1$ and $2u_3$ are the macroscopic shear and normal displacements, respectively, across the faces of the egg-box.

4.2. Numerical simulations of egg-box panel

The finite element simulation for frusta subjected to transverse shear loading was repeated for an elastic-ideally plastic solid with yield strain of 0.3% and Poisson's ratio of 0.3 using the same geometry, finite element mesh, boundary conditions and initial geometric imperfection as described in Section 3 for an elastic/power-law hardening solid.

For completeness, the simulation was repeated for frusta made from an elastic/ideally plastic solid (with yield strain of 0.3% and Poisson's ratio of 0.3) and subjected to axial loading parallel to the x_3 axis. In this case, the base of each frustum was constrained against lateral displacement and rotation. The boundary conditions on the top face of the frustum represented a rigid platen bonded to the top face, with a prescribed axial displacement u_3, and zero radial motion. To mimic this in the finite element simulations, all nodes on the top face of each frustum shared the prescribed axial displacement u_3, with full radial constraint, i.e. $u_1^2 + u_2^2 = 0$. Frictionless contact between the loading platen and the inclined wall of the conical frustum was included in the analysis. These boundary conditions are consistent with those for egg-box panel with bonded face sheets as considered by Zupan et al. [14]. A geometric imperfection was introduced using an axisymmetric eigenmode obtained from a linear perturbation analysis; a typical mode shape is shown in Fig. 11(a) for a frustum with $\omega = 45^\circ$, $a/t = 10$ and $a/h = 0.5$. The axisymmetric

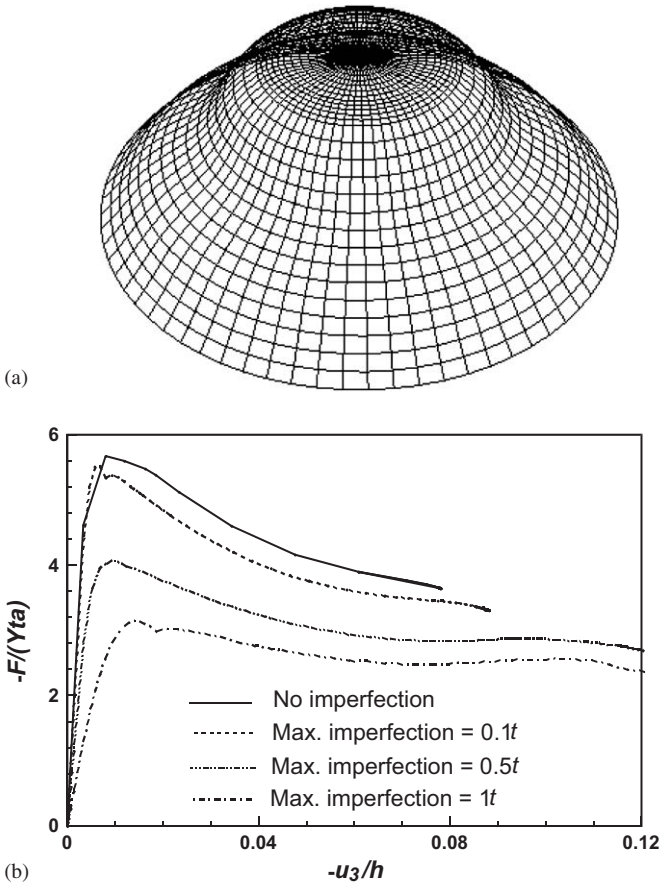

Fig. 11. (a) The eigenmode shape used for introducing geometric imperfection to the conical frusta subjected to compressive normal load. (b) Effect of the magnitude of geometric imperfection on the normal force, F, versus displacement, u_3, response of a conical frustum with cone angle $\omega = 45^\circ$ and wall thickness $t = 0.5$ mm, and made from an elastic/ideally plastic solid with yield strain $\varepsilon_y = 0.3\%$. The normal force has been normalised by Yta where Y is the yield strength of the solid, and the displacement has been normalised by the height h (= 10 mm).

mode shape shown in Fig. 11(a) is similar to the experimentally observed plastic collapse mode for metallic conical frusta subjected to compressive normal load, see for example Deshpande and Fleck [13], Mamalis et al. [2], Mamalis and Johnson [16] and Zupan et al. [14]. The effect of the magnitude of imperfection on the normalised compressive force versus normalised axial displacement response is shown in Fig. 11(b). In contrast to the shear-buckling load, the normal compressive collapse load is sensitive to the magnitude of geometric imperfection. Consider an imperfection such that the maximum transverse distortion is 10% of the wall thickness; then, the normal collapse load is almost equal to that for a perfect frustum. In contrast, the collapse load when the imperfection is 100% of the wall thickness is about 55% that for a perfect frustum. The maximum transverse distortion associated with the imperfection was chosen to be 10% of the wall thickness for all cases of the conical frusta subjected to normal loading considered in this study.

4.3. Stress versus strain response of an egg-box panel

The predicted shear stress τ versus shear strain γ, and normal stress σ versus normal strain ε, responses of the egg-box material made from an elastic/ideally plastic solid are shown in Fig. 12 for a relative density in the range $0.005 \leqslant \bar{\rho} \leqslant 0.052$. The stresses are normalised by the yield strength Y of the solid and are plotted on a logarithmic scale due to the wide range in strengths. The τ versus γ response and the collapse mode shape for the elastic/ideally plastic solid are qualitatively similar to the corresponding shear force versus shear displacement response for an elastic/power-law hardening solid. The predicted shear stress versus shear strain response show an initial peak, corresponding to the initiation of plastic buckling, accompanied by a subsequent drop in load in the post-buckling regime.

Axial compressive loading leads to axisymmetric progressive crushing of the frustum, with axisymmetric buckling starting near the narrow end of the frustum. The oscillations in σ (see Fig. 12(b)) indicate the successive initiation of axisymmetric folds (occurring at peak stress) and then contact between the sides of the fold (at each trough). Similar oscillations in the σ versus ε response have been observed by Zupan et al. [14] in their compressive tests on aluminium alloy egg-box panels with well-bonded face sheets, and by Mamalis et al. [2] in their quasi-static compression tests of aluminium alloy and low-carbon steel frusta.

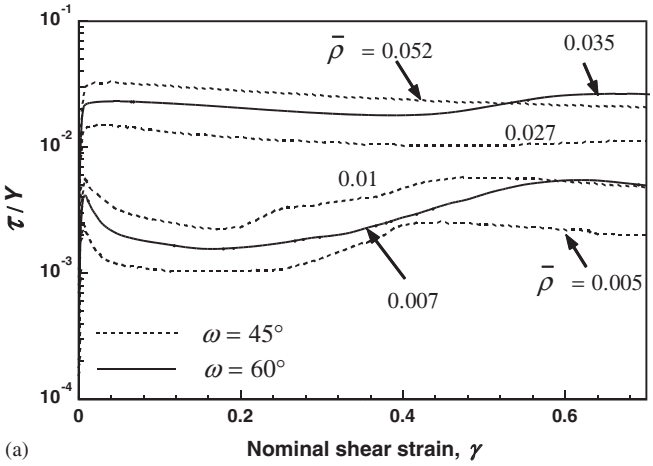

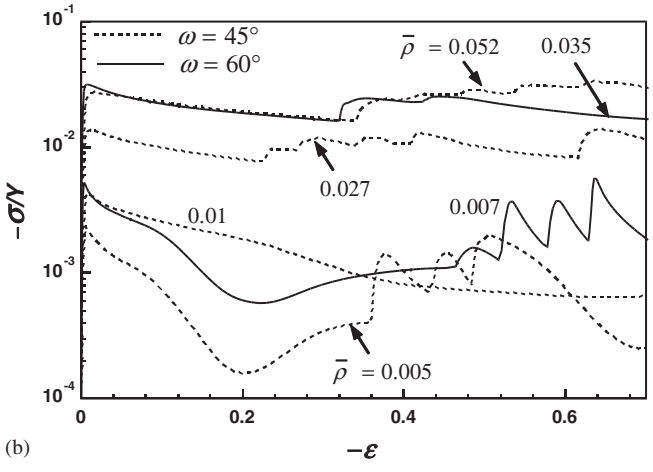

Fig. 12. (a) Shear stress, τ, versus shear strain, γ, and (b) normal stress, σ, versus normal strain, ε, for an egg-box material with a flat top of radius a and a wall thickness t, for relative density in the range $0.005 \leqslant \bar{\rho} \leqslant 0.052$. The stresses have been normalised by the uniaxial yield strength Y of the material. The results are for egg-box panel made from an elastic/ideally plastic solid.

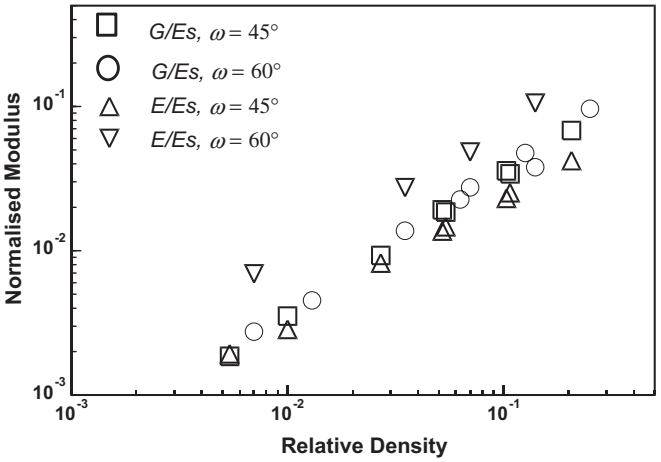

Fig. 13. Normalised modulus versus relative density for an egg-box panel made from an elastic/ideally plastic solid.

The effective shear modulus G/E_s and through-thickness Young's modulus E/E_s of the egg-box material are plotted as a function of the relative density in Fig. 13 where E_s denotes the Young's modulus of the solid. The effective shear modulus of the egg-box material has a negligible sensitivity to the cone angle in the range $\omega = 45^\circ - 60^\circ$. However, the effective Young's modulus E increases with increasing ω. Both G and E scale linearly with relative density $\bar{\rho}$, consistent with the fact that the frusta deform in a stretching rather than in a bending mode.

4.4. Energy absorption characteristics of an egg-box panel

The predicted energy absorbed per unit-enclosed volume of the egg-box material is determined from the area under the macroscopic nominal stress versus nominal strain curve up to a given level of strain. For axial compressive loading, the predictions shown in Fig. 12(b) suggest that densification occurs at a nominal strain of about $\varepsilon = -0.6$, and so the absorbed energy is defined at a nominal strain of $\varepsilon = -0.6$. Now consider the shear response. For the range of relative density considered ($0.005 \leqslant \bar{\rho} \leqslant 0.25$), the conical portion behind the plastic hinge undergoes ductile tearing at a nominal shear strain $\gamma (= u_1/h)$ of between 0.1 and 0.4 (recall the experimentally determined shear force versus shear displacement response shown in Fig. 5; the tests were terminated at the onset of tearing). The predicted energy absorbed by the egg-box material in shear is thereby

defined at a shear strain of $\gamma = 0.1$ and 0.4. The predicted values of initial peak stress and the absorbed energy per unit volume, both normalised by the yield stress of the material, are shown as a function of the relative density in Fig. 14. There is a negligible effect of the cone angle ω (for $\omega = 45^\circ$ and 60°) upon the normalised maximum shear stress versus relative density response, while the normalised maximum normal stress at a given relative density is slightly greater for $\omega = 60^\circ$ than for 45°. Also, the maximum shear stress at a given relative density is comparable to the maximum normal stress. Both the shear strength and the through-thickness collapse strength scale linearly with the relative density. On a practical note, egg-box panels are typically bonded to face sheets, and face sheets may debond at stress levels well below the maximum shear stress at which plastic buckling of the egg-box panel occurs. Careful consideration must be given to the attachment of the face sheets to a metallic egg-box panel in order to ensure maximum energy absorption.

For both shear and normal loadings, there is a negligible effect of the magnitude of the cone angle ω upon the energy absorbed by the egg-box material, see Fig. 14(b). We find that the energy absorbed per unit volume of the egg-box material subjected to normal loading up to $\varepsilon = -0.6$ is comparable to that absorbed by an egg-box material subjected to shear loading up to a shear strain of $\gamma = 0.4$.

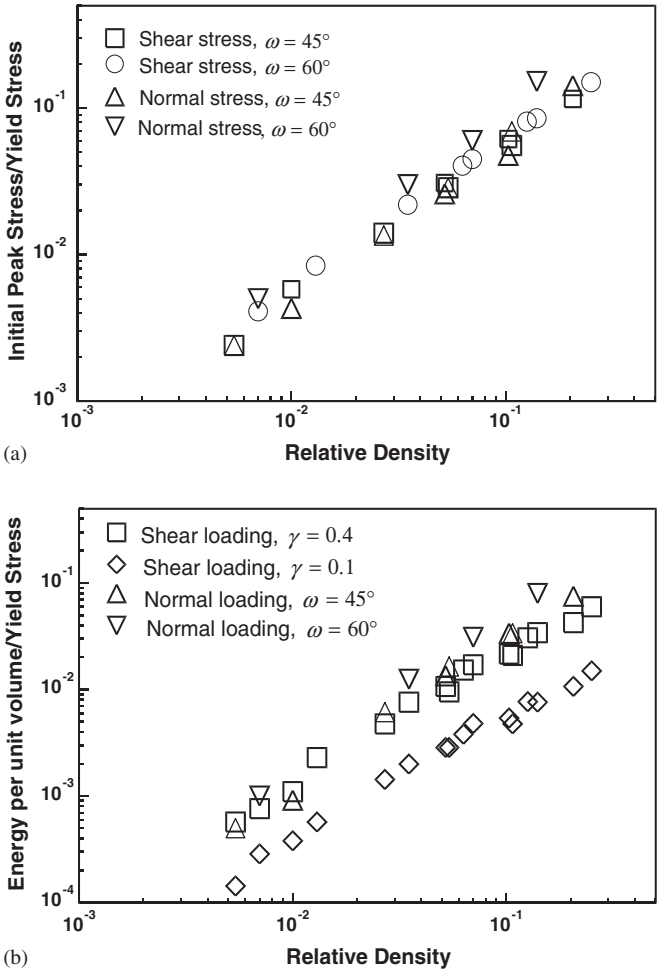

Fig. 14. (a) Initial peak shear stress versus relative density, and (b) energy absorption per unit volume versus relative density of egg-box panel made from an elastic/ideally plastic solid.

4.5. Collapse surface of an egg-box panel

The collapse surface of an egg-box panel made from an elastic-ideally plastic material and subjected to a combination of remote shear and normal loading was also determined. Finite element analysis of the conical frustum has been performed with proportional loading in displacement space. Selected combinations of shear displacement, u_1, and normal displacement, u_3, were applied over the range $0 \leqslant \Phi \leqslant \pi$, where $\Phi = \tan^{-1}(u_1/u_3)$. The limit $\Phi = 0$ corresponds to purely tensile straining while $\Phi = \pi/2$ corresponds to shear loading with no axial displacement. No geometric imperfection was used in the analysis involving combined normal and shear loading, and the initial peak values of shear and normal loads in the plastic collapse of the frustum were used to determine the collapse stresses for an egg-box material. Recall that the normal and shear collapse loads for a "perfect" frustum are not significantly different from the corresponding values for a frustum containing an initial geometric imperfection with a transverse displacement of $0.1t$, where t is the wall thickness, see Figs. 7(b) and 11(b).

The resulting collapse surface for an egg-box material of $\bar{\rho} = 0.027$ is shown in Fig. 15 in $\sigma - \tau$ space (only for $\tau \geqslant 0$). For combined compressive normal and transverse shear loading, the buckling mode is a combination of axisymmetric buckling associated with the normal load (Fig. 11(a)) and the buckling mode associated with transverse shear (see Fig. 7(a)). However, for combined tensile normal and shear loading, the mode is a combination of stretching in the axial direction and the buckling mode associated with shear loading. Note that the collapse surface is almost circular in shape and is symmetric about both the $\tau = 0$ and $\sigma = 0$ axes. Thus, the magnitude of the collapse load for compressive normal loading is equal to that for normal tension suggesting that buckling and plastic yielding occur almost simultaneously in the frustum.

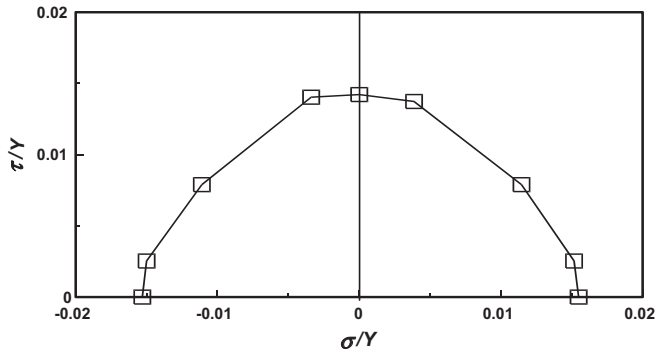

Fig. 15. The collapse surface for an egg-box material of relative density $\bar{\rho} = 0.027$.

The plastic collapse surface for a conical frustum shown in Fig. 15 is qualitatively similar to that for a circular cylindrical shell. The plastic collapse shear stress for a circular cylindrical shell subjected to a combined macroscopic axial stress σ and shear stress τ has been shown to depend on the magnitude and not on the sign of σ/τ, in the range $-1 \leqslant \sigma/\tau \leqslant 1$ [17]. Further, the measured plastic shear collapse load of a circular cylinder, subjected to transverse shear with axial constraint (equivalent to a combination of axial tension and transverse shear), is lower than the shear collapse load without axial constraint [12]; this is consistent with the collapse surface results for egg-box panel as presented in Fig. 15.

5. Concluding remarks

The response of conical frusta to shear loading has been determined by a combination of experiments and finite element simulations. The shear collapse load is weakly dependent on the magnitude of geometric imperfection while the collapse load under normal compressive loading is very sensitive to the magnitude of imperfection. The peak shear load on a conical frustum decreases with increasing cone angle, whereas it increases with increasing wall thickness of the frustum. The energy absorption in shear is limited by the onset of sheet necking in the wall of the frustum; loading beyond the initiation of plastic buckling results in significant stretching of the conical portion of the frustum and to tensile tearing of the material.

Finite element analysis of a conical frustum made from an elastic/ideally plastic solid and subjected to a combination of shear and normal (i.e. axial) loads has been carried out and the results used to predict the collapse response and energy absorption characteristics of an egg-box panel comprising an array of conical frusta. The shear strength and through-thickness collapse strength of the egg-box are comparable, and scale linearly with the relative density. The collapse surface in stress space has been determined for an egg-box panel subjected to a combination of shear and normal loading; the collapse surface is almost circular in shape.

Acknowledgements

The authors are grateful to DARPA/ONR for their financial support. The authors would like to thank Prof. M.F. Ashby, Dr. V. Deshpande and Dr. M. Zupan for helpful discussions, and are grateful to S. Marshall and A. Heaver for help with the experiments.

References

[1] Mamalis AG, Johnson W. The quasi-static crumpling of thin-walled circular cylinders and frusta under axial compression. International Journal of Mechanical Sciences 1983;25(9):713–32.
[2] Mamalis AG, Manolakos DE, Saigal S, Viegelahn G, Johnson W. Extensible plastic collapse of thin-wall frusta as energy absorbers. International Journal of Mechanical Sciences 1986;28(4):219–29.
[3] Bardi FC, Yun HD, Kyriakides S. On the axisymmetric progressive crushing of circular tubes under axial compression. International Journal of Solids and Structures 2003;40:3137–55.
[4] Ashby MF, Evans AG, Fleck NA, Gibson LJ, Hutchinson JW, Wadley HG. Metal foams: a design guide. Boston, MA, USA: Butterworth-Heinemann; 2000.
[5] Reid SR. Plastic deformation mechanisms in axially compressed metal tubes used as impact energy absorbers. International Journal of Mechanical Sciences 1993;35(12):1035–52.
[6] Alghamdi AAA. Collapsible impact energy absorbers: an overview. Thin-Walled Structures 2001;29:189–213.
[7] Mamalis AG, Manolakos DE, Baldoukas AK, Viegelahn GL. Deformation characteristics of crashworthy thin-walled steel tubes subjected to bending. Proceeding of the IMechE Part C: Journal of Engineering Science 1989;203:411–7.
[8] Kecman D. Bending collapse of rectangular and square section tubes. International Journal of Mechanical Sciences 1983;25(9):623–36.
[9] Chen C, Harte A-M, Fleck NA. The plastic collapse of sandwich beams with a metallic foam core. International Journal of Mechanical Sciences 2001;43:1483–506.
[10] Galletly GD, Blachut J. Plastic buckling of short vertical cylindrical shells subjected to horizontal edge shear loads. Journal of Pressure Vessel Technology—Transactions of The ASME 1985;107:101–6.
[11] Matsuura S, Nakamura H, Kokubu S, Ogiso S, Ohtsubo H. Shear-bending buckling analyses of fast breeder reactor main vessels. Nuclear Engineering Design 1995;153:305–17.
[12] Athiannan K, Palaninathan R. Buckling of cylindrical shells under transverse shear. Thin-Walled Structures 2004;42:1307–28.
[13] Deshpande VS, Fleck NA. Energy absorption of an egg-box material. Journal of the Mechanics and Physics of Solids 2003;51:187–208.
[14] Zupan M, Chen C, Fleck NA. The plastic collapse and energy absorption capacity of egg-box panels. International Journal of Mechanical Sciences 2003;45(5):851–71.
[15] ABAQUS/Standard Users Manual, version 6.1, Hibbitt, Karlsson and Sorensen Inc. Providence, Rhode Island, 2001.
[16] Mamalis AG, Johnson W. The quasi-static crumpling of thin-walled circular cylinders and frusta under axial compression. International Journal of Mechanical Sciences 1983;25:713–32.
[17] Mao R, Lu G. Plastic buckling of circular cylindrical shells under combined in-plane loads. International Journal of Solids and Structures 2001;38:741–57.